ELSEVIER

Materials Science and Engineering A357 (2003) 412–422

MATERIALS SCIENCE & ENGINEERING A

www.elsevier.com/locate/msea

Microscopy of wear affected surface produced during sliding of Nimonic 80A against Stellite 6 at 20 °C

H.L. Du [a,*], P.K. Datta [a], I. Inman [a], R. Geurts [b], C. Kübel [b]

[a] *Advanced Materials Research Institute, Northumbria University, Newcastle upon Tyne NE1 8ST, UK*
[b] *FEI Company, Application Laboratory, Eindhoven, The Netherlands*

Received 7 January 2003; received in revised form 19 March 2003; accepted 25 March 2003

Abstract

The microstructures of a wear induced surface glazed layer formed during sliding wear of Nimonic 80A against Stellite 6 at 20 °C using a speed of 0.314 ms^{-1} under a load of 7 N have been investigated using X-ray diffraction analysis, scanning electron microscopy, and transmission electron microscopy in combination with electron energy loss spectroscopy (EELS) and energy dispersive X-ray (EDX) analysis. The results indicate the formation of a wear resistant nano-structured glazed layer. The mechanisms responsible for the formation of the nano-polycrystalline glazed layer are discussed.

Keywords: Wear; Glaze layer; Oxidation; Superalloy; TEM; Nanostructure

1. Introduction

High temperature wear encountered in many situations—power generation, transport, materials processing and nuclear reactors [1–6]—is a serious problem. The fast kinetics of surface oxidation, the loss of mechanical strength of the materials constituting the contacting surfaces and the change in adhesion between these surfaces caused by the joint action of temperature and tribological parameters accentuate the problem of high temperature wear. The conditions associated with high temperature severely restrict the choice of coatings and materials that can be used to prevent/minimise high temperature wear [1–7].

An alternative approach of generating wear resistant surfaces on coated and uncoated materials is to take advantage of the important events—oxidation, debris generation and elemental transfer between the contacting surfaces, which accompany the process of high temperature wear [1,2,7]. These events under certain conditions of temperature, pressure and speed lead to the formation of surface glazes on the contacting surfaces with immunity to further wear [1,2,7]. Although this phenomenon of glaze formation and the general issues relating to wear at elevated temperatures have been the subject of several studies [1,2,8–13] it is still difficult to predict the precise conditions, which promote the formation of glazed surfaces. Determination of such conditions is the key factor in establishing the mechanisms responsible for glaze formation. Bearing this in mind a programme of research involving the studies of high temperature wear of Nimonic 80A and other superalloys has been initiated in our laboratory. The characteristics of this research is that it involved: (i) wear studies on like-on-unlike systems; (ii) with limited debris retention between the contacting surfaces; and (iii) underpinned by extensive transmission electron microscopy of the wear affected surfaces generated.

We reported previously [13] our results from wear studies on Nimonic 80A against Stellite 6 at 750 °C using a speed of 0.314 ms^{-1} under a load of 7 N. The results demonstrated the formation of nanostructured wear resistant surfaces. The mechanisms for the formation of nanostructured surface and the way such surfaces develop their wear resistance were discussed.

We have now extended this study to other temperatures. In this paper we report the results obtained from

* Corresponding author. Tel.: +44-191-227-4973; fax: +44-191-227-3598.
E-mail address: hailiang.du@unn.ac.uk (H.L. Du).

0921-5093/03/$ - see front matter
doi:10.1016/S0921-5093(03)00258-2

wear studies at 20 °C and compare the results with those obtained at other temperatures (~750 °C).

2. Experimental

2.1. Wear testing

All high temperature wear tests were carried out in a high temperature reciprocating wear rig. Details of the high temperature wear machine used have been described previously [1,2,13] and only a brief description is presented here. Basically the machine was a block-on-cylinder arrangement—the cylinder being the counterface and the block being the sample. A variable speed electric motor allowed the attached shaft to rotate the counterface mounted on the shaft at various speeds. In the present work samples of Nimonic 80A of dimensions $5 \times 5 \times 45$ mm^3 were held against the counterface made of Stellite 6 of diameter 50 mm and length 50 mm. The wear test parameters included load of 7 N, speed of 0.314 ms^{-1} and temperatures of 20 °C. The chemical compositions of Nimonic 80A and Stellite 6 are given in Table 1.

2.2. Characterisation of the wear affected surface using SEM and TEM

2.2.1. SEM analysis

The surface of the bulk sample was analysed using a Hitachi-2400 scanning electron microscope (SEM). The elemental analysis was performed with a FEI Sirion SEM using an acceleration voltage of 10 kV and an Energy dispersive X-ray (EDX) detector with a S-UTW window.

2.2.2. TEM specimen preparation

The cross-sectioned samples for transmission electron microscopy (TEM) analysis were prepared using a FEI Strata DB 235M dual beam focused ion mill (FIB). The wear affected surface of the bulk sample was coated with a thin protective layer of platinum before TEM lamellae were cut using a 30 kV gallium ion beam. Thin TEM windows of about 100-nm thickness were prepared and final polishing was done with a current of 10 nA.

The TEM lamellae were lifted out with a glass needle and placed on carbon coated copper grids for further TEM analysis.

2.2.3. TEM analysis

The TEM analysis of the wear-affected surface was performed using a Tecnai G^2 F20 SuperTwin at 200 kV with a Schottky Field Emitter (FEG). The microscope was fully equipped for analytical work with an energy-dispersive X-ray (EDX) detector with a S-UTW window, a Gatan Imaging Filter (GIF 2000), and a high angle annular dark-field (HAADF) detector for STEM imaging. Unless stated otherwise, the scanning transmission electron microscopy (STEM) imaging and all analytical work were performed with a probe size of 1 nm resulting in a beam current of about 0.5 nA.

TEM images and selected area diffraction (SAD) patterns were collected on a retractable Gatan 794 CCD camera and processed with Digital Micrograph Version 3.6.4. The HAADF-STEM EELS/EDX and CCD line traces were collected fully automatically using the Tecnai G^2 User Interface and processed with the Tecnai Imaging and Analysis (TIA) software Version 1.9.162. All line traces were collected at a specimen tilt-angle of 0°. EDX quantification was performed with spectra collected at a tilt-angle of 15° using TIA; the background correction was done using a polynomial fit and k-factors were calculated theoretically based on the detection geometry and detector properties.

3. Results

3.1. Wear data

Fig. 1 shows the wear data for the Nimonic 80A/Stellite 6 system as a function of temperature obtained from tests carried out under a load of 7 N at a speed of 0.314 ms^{-1}. Weight changes were extremely low for all temperatures. The wear data at 570 °C shows a departure from the general trend.

3.2. Scanning electron microscopy (SEM)

Fig. 2 shows the surface developed at 20 °C. The top glaze layer consisted of a loosely bound uncompacted oxide layer. This layer was easily detachable by brushing or light polishing. The existence of this loosely bound oxide layer was confirmed by optical and scanning electron microscopy. Underneath this loosely bound layer existed a more compacted layer.

Table 1
Nominal compositions of alloys in wt.%

	Fe	Ni	Cr	Al	Ti	Mn	W	Co	Si	C
Stellite 6	2.5 max	2.5 max	27	–	–	1	5	60	1	1
Nimonic 80A	0.7	75.8	19.4	1.4	2.5	–	–	–	0.1	0.08

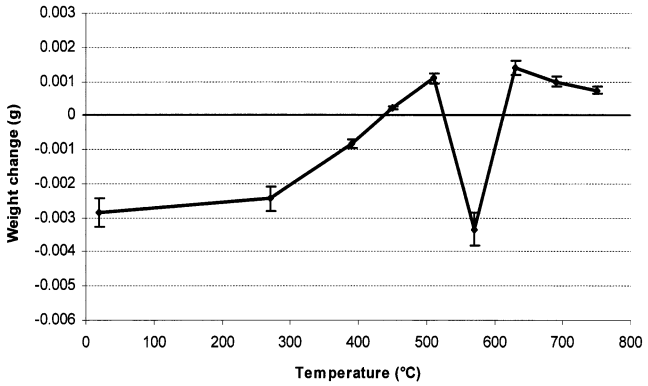

Fig. 1. Weight change versus temperature for sliding Nimonic 80A against Stellite 6.

The composition analysis of the surfaces generated at 20 °C demonstrates the presence of oxygen and of the elements from Nimonic 80A and Stellite 6. The information presented indicates elemental transfer from the counterface to the specimen and mixing of the transferred and host element/oxides. In this paper attention is focussed mainly on the surface layer produced at 20 °C. Some information on the surface layers produced at 750 °C is given for comparison purposes.

3.3. Transmission electron microscopy (TEM)

Fig. 3a shows a cross-sectional TEM overview image of the wear affected Nimonic 80A surface produced by sliding against Stellite 6. It reveals the interface between the Nimonic 80A substrate and the compact glaze layer, whereas the loosely bound uncompacted oxide layer was not visible in this area. The associated selected area diffraction (SAD) pattern (Fig. 3c) is dominated by Debye rings and some well-defined Bragg reflections. Dark-field images (Fig. 3e and f) reveal, that the well-defined reflections correspond to irregular shaped and bend Nimonic 80A crystals of several hundred nanometer diameter, which were observed in a layer up to about ~1 micron from the interface between the glaze layer and Nimonic 80A substrate. In contrast, the glaze layer shows a very different morphology consisting of small and misoriented crystals due to fragmentation. This is clearly revealed by the dark-field images in Fig. 3b–e, which show particles with a typical diameter of 5–20 nm. Although the adhesion between the glaze layer and Nimonic 80A substrate was generally good the formation of cracks in some areas was visible.

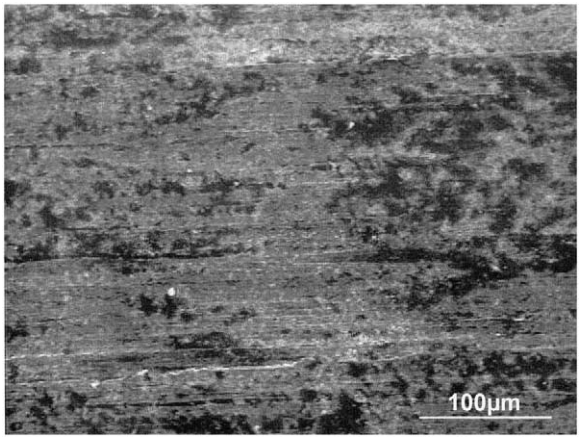

Fig. 2. SEM morphology of worn surface of Nimonic 80A versus Stellite 6 at 20 °C.

Fig. 4 shows a HAADF-STEM overview image of the FIB prepared cross-section analysed in the previous paragraph. The HAADF-STEM image is in good agreement with the structural variations observed by TEM. Two different areas are revealed for the Nimonic 80A—a uniform 'bulk' area as well as large grained structure about one micron below the interface with the glaze layer. The glaze layer exhibits a fine-grained structure (5–20 nm) with irregular shaped grain boundaries. The particle sizes are observed to be larger close to the interface (up to about 50 nm). Furthermore, the strong Z-dependence of the HAADF-STEM image reveals several heavy metal particles in the (oxidized) glaze layer as well as low-density material at the interface.

Fig. 5 shows several examples from a STEM line trace of nano-diffraction patterns with a probe size of about 30 nm. In agreement with the earlier studies, only small randomly oriented crystals are observed in the glaze layer and at the interface. The larger grains in the alloy exhibit various crystallographic orientations; some of them well defined and similar to those expected for Nimonic 80A.

Fig. 6 shows the results of the EDX analysis of the glaze layers together with their reference areas. The quantification is based on theoretical k-factors and uses a thickness correction for an estimated sample thickness of 150 nm (EELS thickness measurements indicate a thickness of 2–3 mean free path). The compositional analysis of the Nimonic 80A layer (area 1) shows the characteristic elements for Nimonic 80A substrate. Quantification of the results reveals a very similar composition as for bulk Nimonic 80A (Table 2). The only difference is a slightly higher silicon concentration and a small amount of cobalt observed in the wear tested material.

The compositional analysis of the glaze layer shows the main elements of Stellite 6 and in addition also a large amount of oxygen and nickel as well as traces of the other elements in Nimonic 80A. Quantification shows that the glaze layer is oxidized Stellite 6 with a significant amount (15–20)% Ni of Nimonic 80A.

The interface layer consists of a mixture of Nimonic 80A and Stellite 6 with a higher than average titanium concentration. Further details are revealed by HAADF-STEM EELS/EDX line traces across the interface as

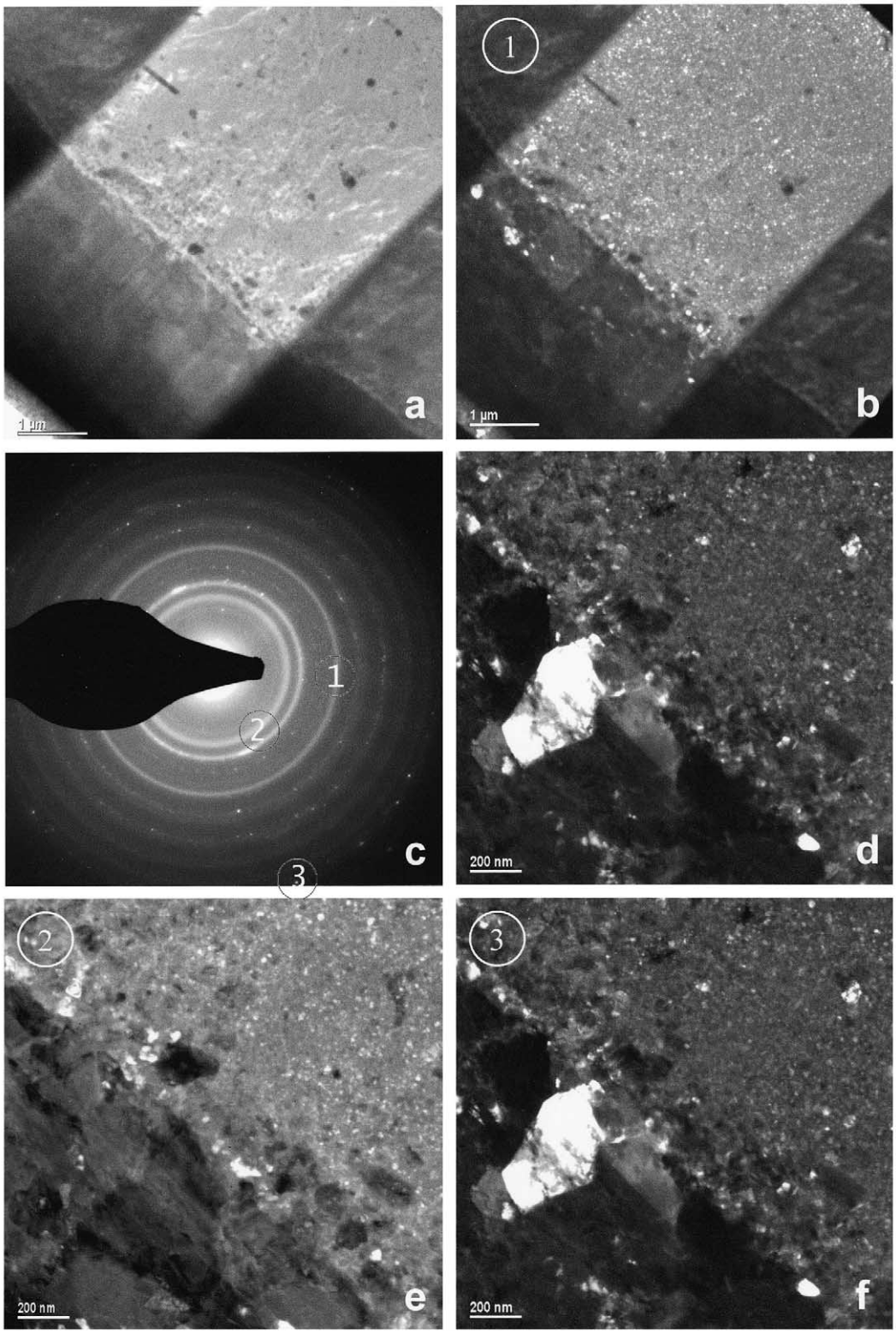

Fig. 3. TEM overview of a cross-section of the wear affected surface: (a) bright-field overview image of the Nimonic 80A and the glaze layer; (b) dark-field image of the nano-crystalline glaze layer (obtained with a 10 micron objective aperture as indicated in the SAD pattern by (1)); (c) selected area diffraction (SAD) pattern of the cross-section; (d) bright-field image of the interface; (e) dark-field image of the nano-crystalline glaze layer close to the interface (as indicated in the SAD pattern by (2)); (f) dark-field image of a larger crystal in the Nimonic 80A close to the interface (as indicated in the SAD pattern by (3)).

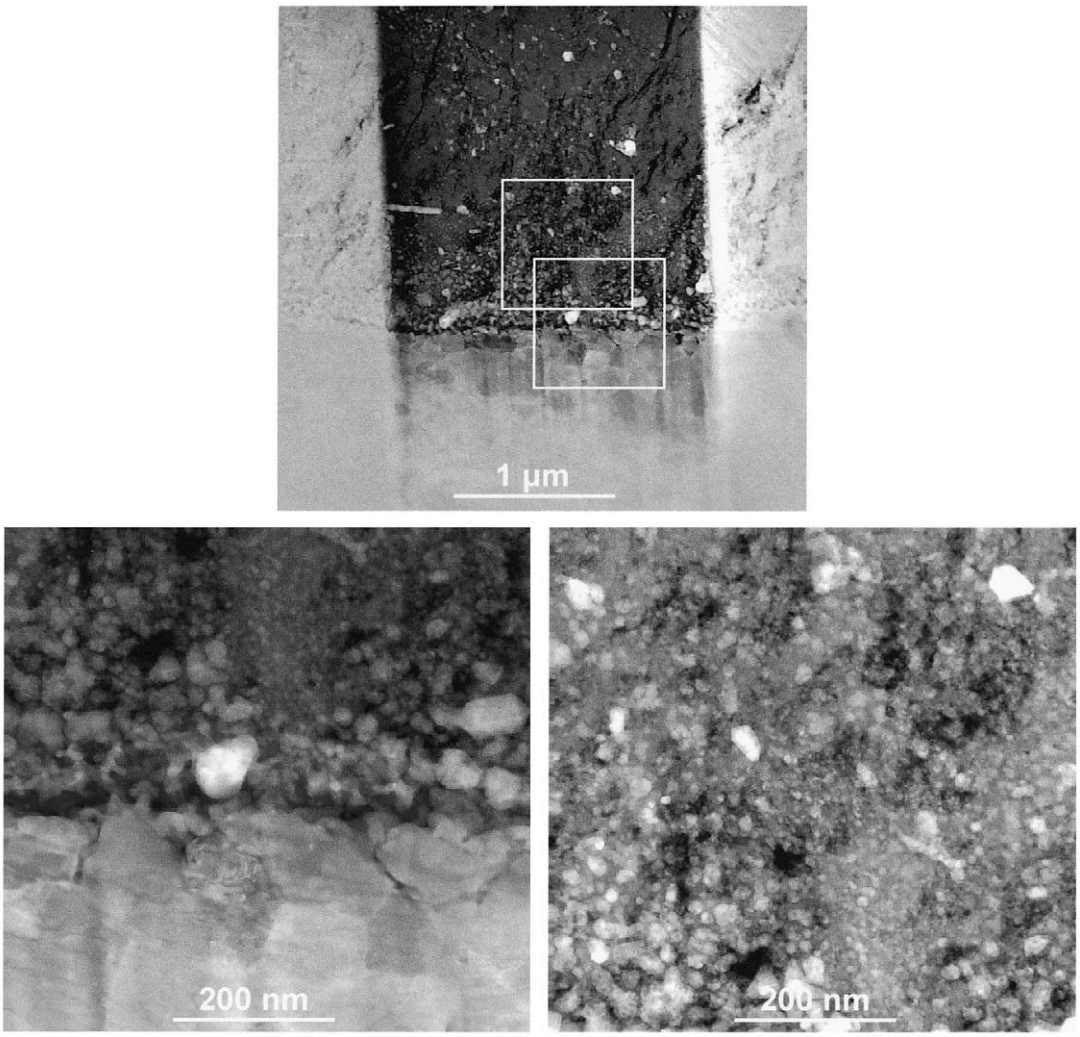

Fig. 4. HAADF-STEM (200 mm camera length) overview image and close-up of the interface and the nano-crystalline glaze layer.

shown in Fig. 7. The line traces show the transition between the glaze layer and the Nimonic 80A based on the cobalt and nickel concentrations. The composition of the glaze layer is locally inhomogeneous as the line traces as shown in Figs. 7 and 8. There is some variation in the chromium, cobalt and oxygen concentrations as well as distinct particles with a high nickel concentration. Nevertheless, the overall concentrations are quite uniform throughout the glaze layer, e.g. no gradient in the nickel concentration was observed. The line traces further reveal the preferential formation of titanium and aluminium oxides in a $\sim$100 nm thick layer at the interface. Slight chromium depletion is observed in the Nimonic 80A substrate close to the interface, which leads to a chromium enrichment in the first $\sim$300 nm of the glaze layer. This has been confirmed independently for several different areas along the interface and can be seen with a higher spatial resolution in the line trace in Fig. 8. Furthermore, the line trace also reveals aluminium enrichment at the interface. From several independent line scans, it has been confirmed that this Al_2O_3 layer is between the TiO_2 layer and the Nimonic 80A substrate. Aluminium (in Al_2O_3) enrichment is further responsible for the dark areas in HAADF-STEM leading from the interface into the top of the Nimonic 80A substrate as illustrated in Fig. 9. Thus it appears that the TiO_2/Al_2O_3 layer represented by the dark lines extended several nanometers along the interface although interrupted at several points as indicated by scans in these locations.

The atomic numbers of chromium (24), cobalt (27) and nickel (28) are quite similar and compositional variations of these main elements do not explain the strong contrast observed in the HAADF-STEM image. However, the EDX/EELS line traces reveal a low oxygen concentration for the bright areas in HAADF-STEM, indicating that the image mostly reflects the oxidation state (which changes the average atomic number/materials density). Furthermore, the low oxygen concentration seems to coincide with a low chro-

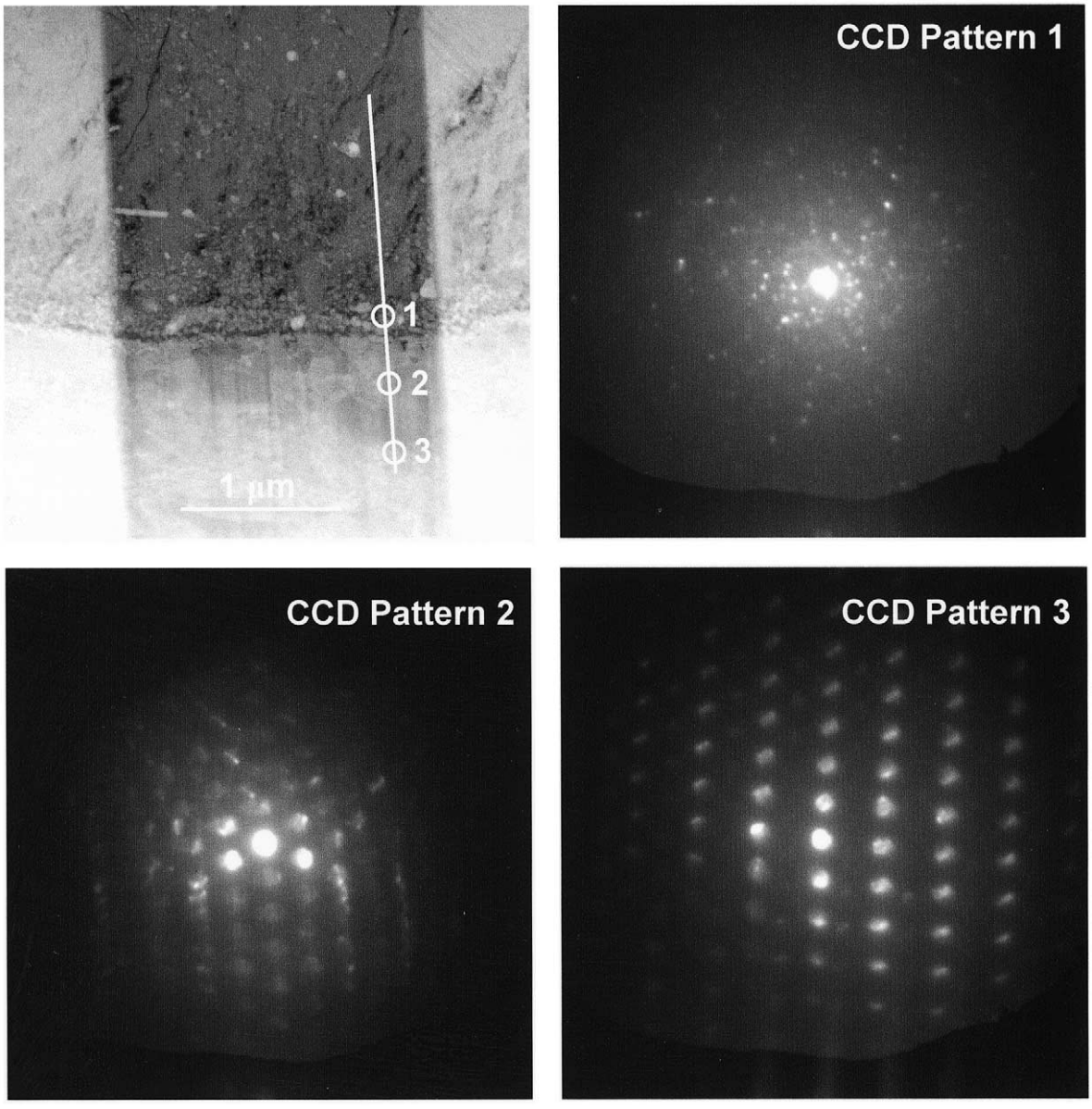

Fig. 5. HAADF-STEM overview image with examples from a CCD line trace.

mium concentration. This has been confirmed by local EDX analysis, which shows a low chromium and oxygen concentration for the particles that appear bright in HAADF-STEM. This implies that some of the nickel and cobalt particles are not completely oxidised.

The overall composition of the Nimonic 80A is quite uniform. However, EDX line traces in an area up to about one micron below the interface reveal the preferential segregation of light elements, especially aluminium and in some cases also titanium (Fig. 10). This segregation is also visible in the HAADF-STEM images as thin lines (<10 nm diameter) oriented preferentially parallel to the interface (Figs. 4, 9 and 10). It is noted that the peaks of Ti and Al are overlapped away from the interface, which indicates the presence of γ'-phase, Ni_3Al or $Ni_3(TiAl)$. The precipitation of intra-granular sub-microscopic of γ'-phase, $Ni_3(TiAl)$ in Nimonic 80A by age hardening is well documented [14].

4. Discussion

The present results clearly indicate the formation of a wear resistant nanostructured surface during the sliding wear test of Nimonic 80A against Stellite 6 at 20 °C using a speed of 0.314 ms^{-1} under a load of 7 N. The SEM and TEM analyses reveal the complex structure of this surface consisting of multiple layers:

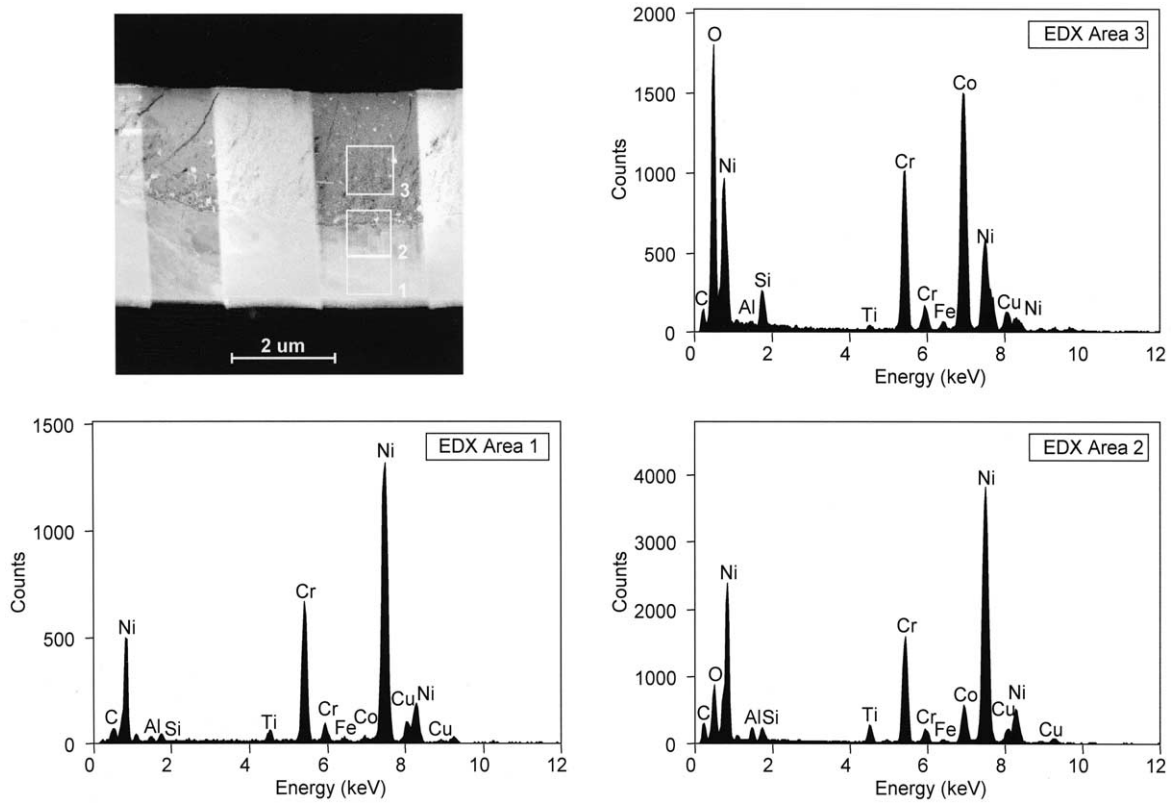

Fig. 6. HAADF-STEM (200 mm camera length) overview image and local EDX analysis.

Table 2
Quantification of the EDX spectra in Fig. 6

Element	Area 1 (Nominic 80A substrate)		Area 3 (Glaze layer)	
	wt.%	at.%	wt.%	at.%
Al	0.7	1.4	0.4	0.9
Si	0.7	1.3	1.1	2.3
Ti	1.8	2.1	0.4	0.5
Cr	18.7	20.2	25.0	27.4
Fe	0.7	0.7	1.4	1.4
Co	1.0	0.9	49.8	48.2
Ni	76.6	73.4	19.0	18.4
W	–	–	2.9	0.9

1) A loose, uncompacted, highly oxidized layer
2) A nano-crystalline (5–20 nm grain diameter) compacted layer mostly consisting of oxides of elements originating both from Stellite 6 and Nimonic 80A. The nickel concentration (from the Nimonic 80A) is uniform throughout the whole layer, except for the presence of several larger non-oxidized particles that were randomly dispersed in the glaze.
3) Larger particles with a diameter of up to 50 nm were observed in a layer of about 300 nm at the bottom of the glaze layer. The compositions indicate the presence of elements from both Stellite 6 and Nimonic 80A, but chromium enriched.
4) The chromium rich phase was gradually transited into a titanium (oxide) rich phase of about 100 nm thickness, followed by an aluminium (oxide) rich phase of about 50 nm thickness, which formed the interface to the Nimonic 80A substrate.
5) Next to the interface of the glaze layer, the Nimonic 80A substrate exhibited a large-grained structure (several hundred nanometer diameter). Slight chromium depletion was observed. The precipitation lines (diameter <10 nm) were aluminium, and in some cases also titanium, enriched phases formed near the large-grained structures. The larger dark areas perpendicular to the interface were also due to aluminium enrichment.
6) The uniform 'bulk' Nimonic 80A was observed more than one micron below the interface.

The first key process in the development of nanostructured glaze layer involved oxidation of the contacting surface/particles subjected to high mechanical stress and rotational speed. The glaze layer consisting mainly of the oxides of the elements originating from the contacting surface acted as a barrier separating the substrate from the environment. Although the mechanical effect would continue to influence the formed glaze layer and the subsurface deformation, the subsequent oxidation process was controlled by the diffusion of the oxygen species and the substrate elements and the

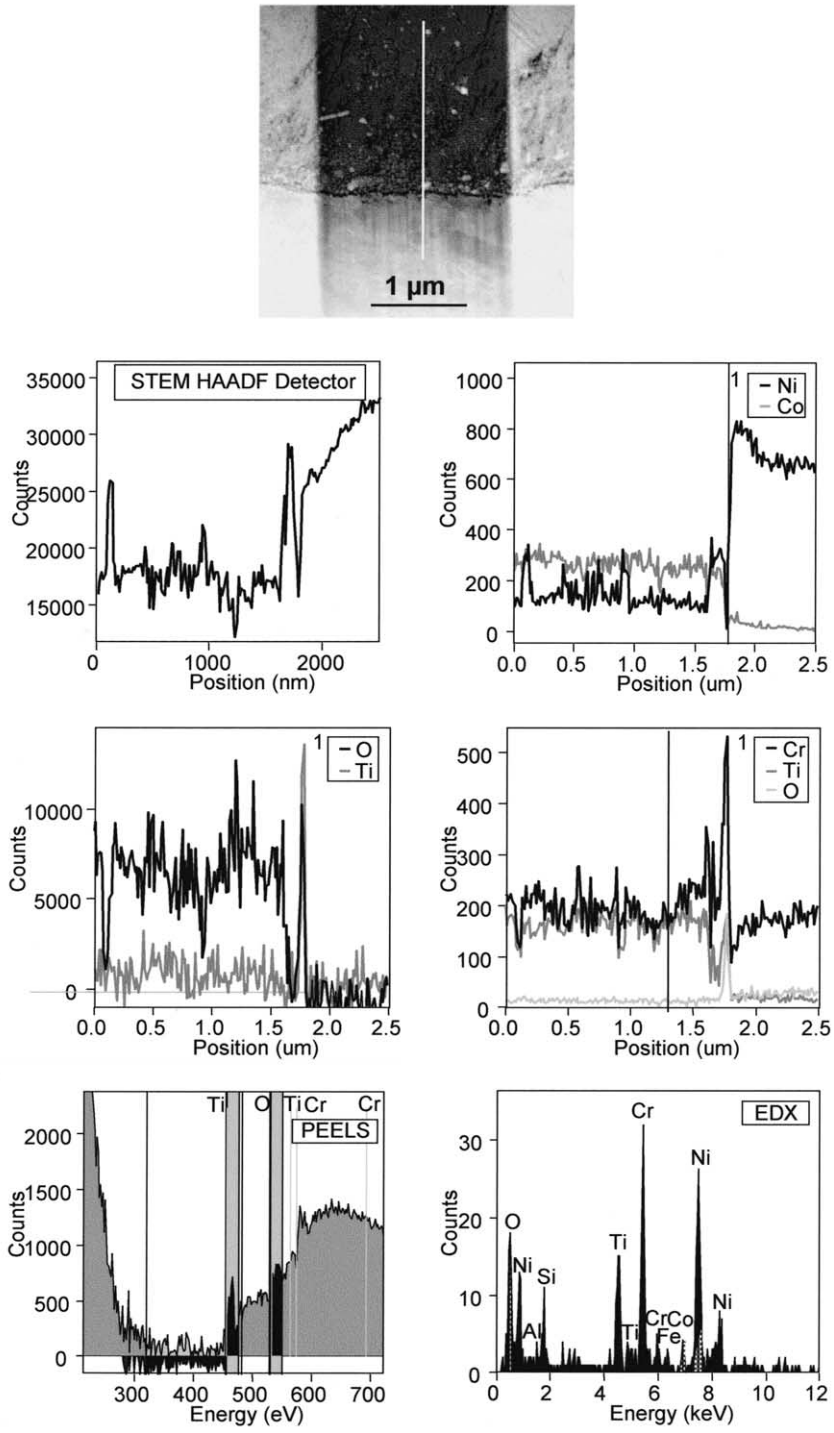

Fig. 7. HAADF-STEM EELS/EDX line trace revealing the compositional variations of the wear affected surface. The line trace was performed with a 1 nm probe size and spectra collected every 10 nm.

thermodynamic nature of the relevant oxides. The observed sequential existence of the oxides Cr_2O_3/TiO_2/Al_2O_3/substrate at the interface can be understood in terms of thermodynamics. Fig. 11 indicates the oxidation tendencies of relevant elements. The dissociation partial pressures for Al_2O_3, TiO_2, Cr_2O_3, NiO and Co_3O_4 follow the same trend in the range of temperatures 25–1000 °C. Al_2O_3, TiO_2 and Cr_2O_3 are more likely to develop with increasing temperatures. Although the temperature generated was not measured, the relatively fast kinetics of oxidation as evidenced by the rapid formation of glaze layer indicates the generation of relative high temperature sufficient for the oxidation process to occur.

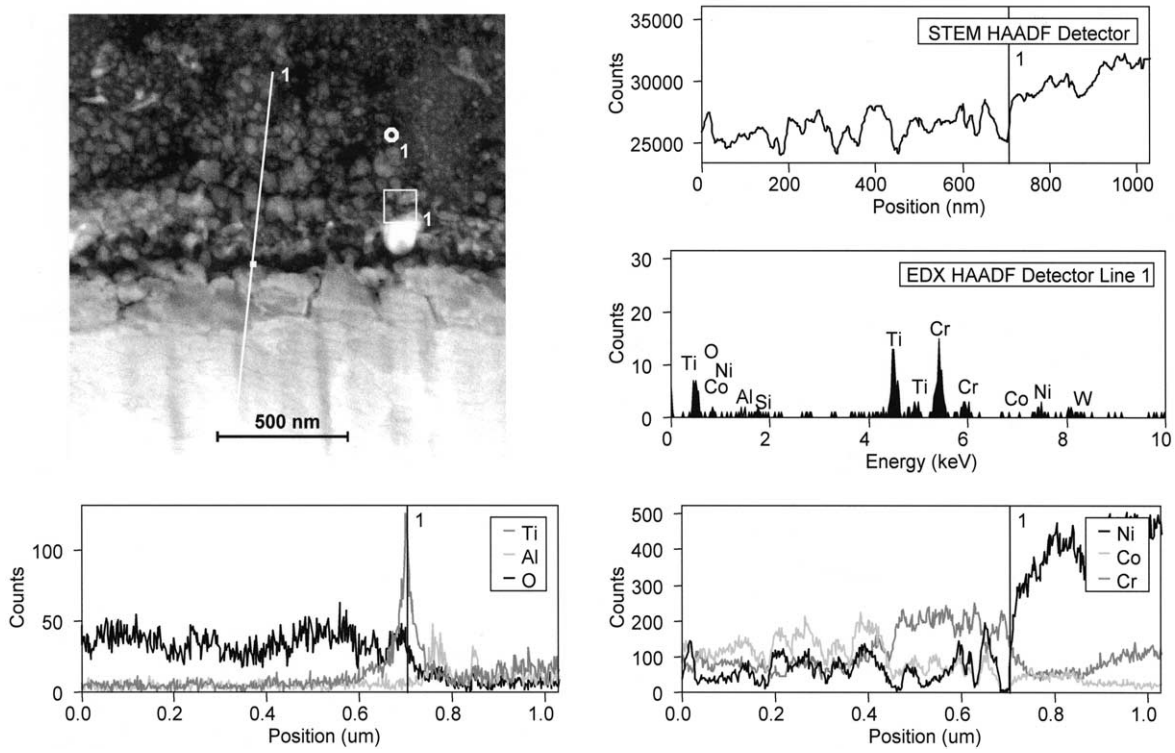

Fig. 8. HAADF-STEM (200 mm camera length) overview and EDX line trace revealing the compositional variations of the interface structure. The line trace was performed with a 1 nm probe size and spectra collected every 2 nm.

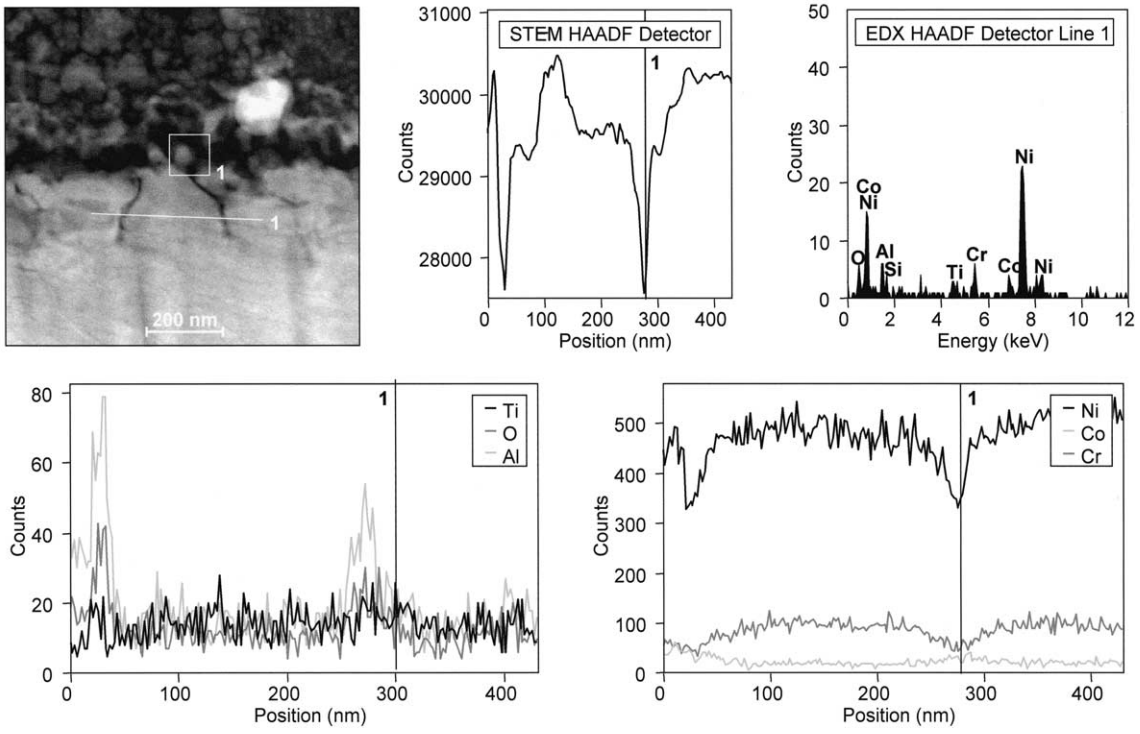

Fig. 9. HAADF-STEM (50 mm camera length) overview and EDX line trace revealing the aluminium (oxide) segregation at the top of the Nimonic 80A phase. The line trace was performed with a 1 nm probe size and spectra collected every 2 nm.

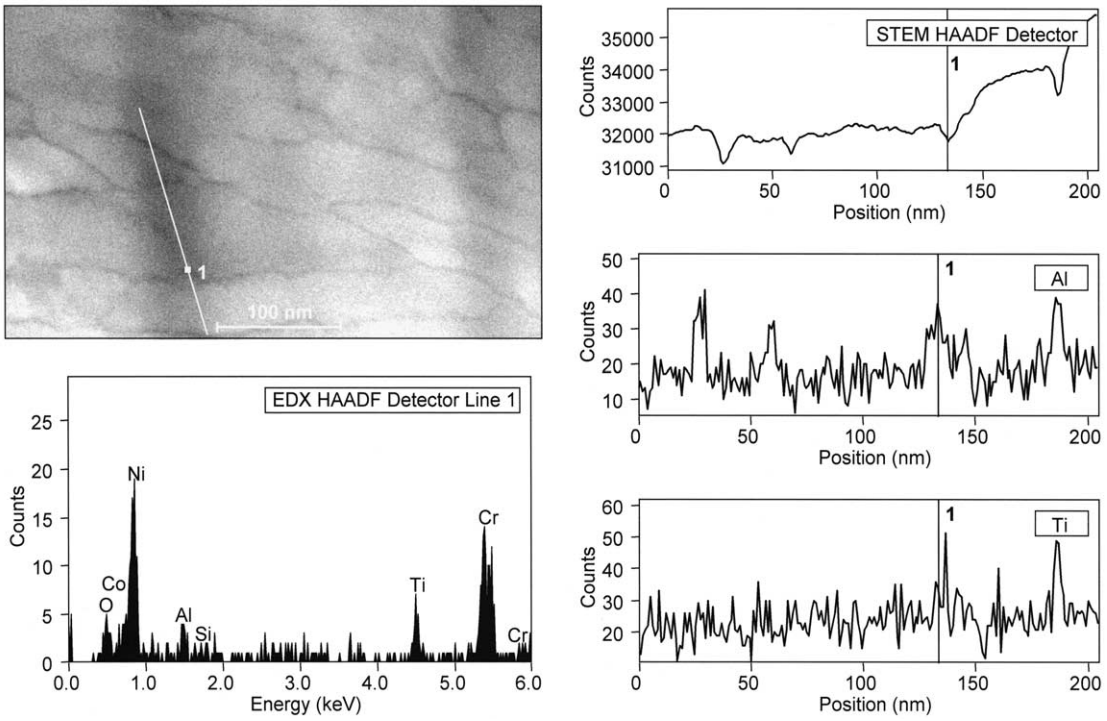

Fig. 10. HAADF-STEM (50 mm camera length) overview and EDX line trace revealing the precipitation of light elements (aluminium and titanium) in the Nimonic 80A close to the interface.

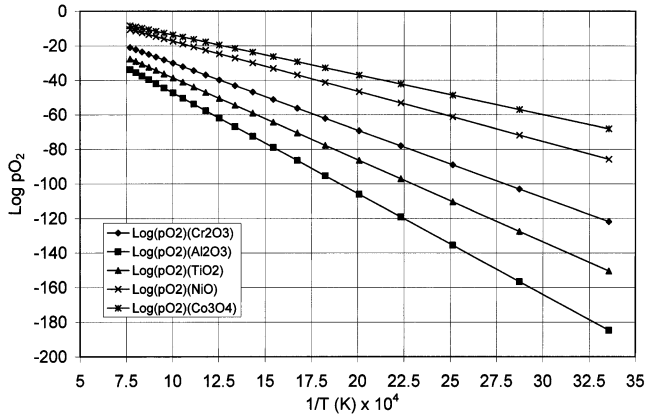

Fig. 11. Dissociation partial pressures of Al_2O_3, TiO_2, Cr_2O_3, NiO and Co_3O_4 versus reciprocals of temperatures.

Additionally, it is apparent that the high Cr activity in both counterface and sample materials leads to the formation of Cr_2O_3 preferentially at the early stages of the process. When oxygen diffuses inward to γ' phase Ti is favourably oxidised. The development of TiO_2 gives rise to the reduction of Ti activity and correspondingly the Al activity increases in the γ' phase and Al_2O_3 becomes a favourable product. Such oxidation mechanisms were observed in the oxidation of TiAl in air in the range of temperatures of 750–950 °C [15]. From the thermodynamic point of view, NiO and Co_3O_4 are much less stable than TiO_2 and Al_2O_3 as shown in Fig. 11, which attributes the fact that some particles of Ni and Co have not been oxidised in the wear process. The oxides—TiO_2 and Al_2O_3—formed beneath the glaze layer play an important role in providing support, additional to that provided by the substrate, to sustain the glaze layer preventing it from collapse [2].

Now the formation of a nanostructured surface and its effectiveness in conferring wear resistance are the two main issues that need consideration and elaboration. Previous work [1,3,13] has demonstrated that sliding wear at 750 °C also generates nanostructured surfaces in the same system under similar tribological parameters. Clearly the nature of the nanostructured surfaces generated at 750 and 20 °C will differ. Nevertheless the formation of nanostructured surfaces at 20 °C can be understood, in a general way, in terms of the mechanisms [13] that were used to explain the formation of similar surfaces at 750 °C. The initial events responsible for generating the glaze layer involve intermixing of the debris generated from the contacting surfaces, oxidation, further mixing (the lack of any composition gradient in the glaze layer indicates efficient intermixing of the components constituting the layer), repeated welding and fracture and final consolidation. The next step involves deformation of the oxides and generation of dislocations leading to the formation of sub-grains. Then occurs further refinement of these sub-grains giving nanostructured grains with high angle boundaries. High internal stress is created inside the grains—dislocation density and arrangement depending on the grain size [16–20]. It appears that in essence these

mechanisms were also operative in the development of wear affected surfaces with nanosized grains at 20 °C.

The significant differences between the situations at 20 and 750 °C were in the rate and degree of the consolidation processes involved in developing the nanostructured glaze layer. Higher temperature allows enhanced diffusion influencing the processes of oxidation, mixing, welding and deformation and fracture of oxides leading to the formation of a highly consolidated glaze layer. Although such a high degree of consolidation was not attainable at 20 °C, as evidenced by the existence of a loose layer at the surface (subsequently removed during the preparation of TEM samples) and a larger interface region, the generation of a nanostructured glaze layer did occur at 20 °C probably aided by the expected higher temperature generated by the wear process itself.

The wear resistance of this surface was reasonable and can be ascribed to the properties of nanostructured surface such as improved toughness, absence of Hall–Petch softening [21] and lack of significant degree of work hardening because of the difficulties in generating dislocation in nanostructured grains [22]. The somewhat inferior wear resistance of this surface compared to that produced at 750 °C, is suggested, was due to the improperly consolidated surface created at 20 °C.

The present observations are encouraging. Further detailed studies of the structure and wear behaviour of the generated surfaces at 20 °C and other temperatures are the subject of other papers. It seems that such information will allow clarification of the mechanisms of glaze formation further and its role in providing wear resistance. It would then be possible to design materials and coatings with enhanced wear performance.

5. Summary

The sliding wear of Nimonic 80A against counterface alloy, Stellite 6, at 20 °C allowed the development of a wear resistant nano-structured glaze layer. The improved wear resistance of such a layer has been attributed to the absence of Hall–Petch softening and the lack of significant degree of work hardening and enhanced fracture toughness of the surface.

Acknowledgements

Grateful acknowledgment to the UK Engineering Physics Science Research Council (EPSRC) is given for financial support to this project.

References

[1] P.D. Wood, PhD Thesis, The Effect of the Counterface on the Wear Resistance of Certain Alloys at Room Temperature and 750 °C, Northumbria University, UK, 1997.
[2] S. Rose, PhD Thesis, Studies of the High Temperature Tribological Behaviour of Some Superalloys, Northumbria University, UK, 2000.
[3] F.H. Stott, D.S. Lin, G.C. Wood, Corrosion Science 13 (1973) 449.
[4] M. Johnson, P. Moorhouse, J.R. Nicholls, DTI Industry Valve Project, 61–68, 1990.
[5] J.-N. Aoh, J.-C. Chen, Wear 250–251 (2001) 611.
[6] J. Singh, A.T. Alpas, Metallurgical and Materials Transactions A 27A (1996) 3135.
[7] F.H. Stott, J. Glascott, G.C. Wood, Wear 97 (1984) 93.
[8] M.G. Gee, N.M. Jennett, Wear 193 (1996) 133.
[9] P.D. Wood, P.K. Datta, J.S. Burnell-Gray, N. Wood, Materials Science Forum 251–254 (1997) 467.
[10] A. Wisbey, C.M. Ward-Close, Materials Science and Technology 13 (1997) 349.
[11] J. Jiang, F.H. Stott, M.M. Stack, Wear 203–204 (1997) 615–625.
[12] X.Y. Li, K.N. Tandon, Wear 245 (2000) 148–161.
[13] S. Datta, I. Inman, H.L. Du, Q. Luo, Microscopy of glazed layers formed during high temperature wear, Invited Talk at the Institute of Materials, Tribology Meeting, London, November, 2001.
[14] W. Betteridge, J. Heslop, The Nimonic Alloys, Edward Arnold (Publishers) Limited, London, 1974.
[15] H.L. Du, A. Aljarany, P.K. Datta, J.S. Burnell-Gray, Oxidation behaviour of Ti–46.7Al–1.9W–0.5Si in air and Ar–20%O_2 between 750 and 950 °C, to be published.
[16] H. Gleiter, Progress in Materials Science 33 (1989) 223.
[17] R.Z. Valiev, R.K. Islamgalier, I.V. Alexandrov, Progress in Materials Science 45 (2000) 103.
[18] T.C. Lowe, R.Z. Valiev, JOM 52 (2000) 27.
[19] A.K. Ghosh, W. Huang, in: T.C. Lowe, R.Z. Valiev (Eds.), Investigations and Applications of Severe Plastic Deformation, Kluwer Academic Publications, 2000, p. 29.
[20] R.S. Mishra, S.X. McFadden, A.K. Mukherjee, Materials Science Forum 304–306 (1999) 31.
[21] R.S. Mishra, A.K. Mukherjee, in: A.K. Ghosh, T.R. Bieler (Eds.), Superplasticity and Superplastic Forming, TMS Warrendale, 1998, p. 109.
[22] R.S. Mishra, S.X. McFadden, A.K. Mukherjee, in: T.C. Lowe, R.Z. Valiev (Eds.), Investigations and Applications of Severe Plastic Deformation, Kluwer Academic Publications, 1994, p. 231.